Optical and x-ray alignment approaches for off-plane reflection gratings

Ryan Allured, Benjamin D. Donovan, Casey T. DeRoo, Hannah R. Marlowe, Randall L. McEntaffer, et al.

Ryan Allured, Benjamin D. Donovan, Casey T. DeRoo, Hannah R. Marlowe, Randall L. McEntaffer, James H. Tutt, Peter N. Cheimets, Edward Hertz, Randall K. Smith, Vadim Burwitz, Gisela Hartner, Benedikt Menz, "Optical and x-ray alignment approaches for off-plane reflection gratings," Proc. SPIE 9603, Optics for EUV, X-Ray, and Gamma-Ray Astronomy VII, 960315 (4 September 2015); doi: 10.1117/12.2186412

SPIE.

Event: SPIE Optical Engineering + Applications, 2015, San Diego, California, United States

Optical and X-ray Alignment Approaches for Off-Plane Reflection Gratings

Ryan Allured[a], Benjamin D. Donovan[b], Casey T. DeRoo[b], Hannah R. Marlowe[b], Randall L. McEntaffer[b], James H. Tutt[b], Peter N. Cheimets[a], Edward Hertz[a], Randall K. Smith[a], Vadim Burwitz[c], Gisela Hartner[c], Benedikt Menz[c]

[a]Harvard-Smithsonian Center for Astrophysics, Cambridge, MA, USA
[b]University of Iowa, Iowa City, IA, USA
[c]Max-Planck-Institut für extraterrestrische-Physik, Garching, Germany

ABSTRACT

Off-plane reflection gratings offer the potential for high-resolution, high-throughput X-ray spectroscopy on future missions. Typically, the gratings are placed in the path of a converging beam from an X-ray telescope. In the off-plane reflection grating case, these gratings must be co-aligned such that their diffracted spectra overlap at the focal plane. Misalignments degrade spectral resolution and effective area. In-situ X-ray alignment of a pair of off-plane reflection gratings in the path of a silicon pore optics module has been performed at the MPE PANTER beamline in Germany. However, in-situ X-ray alignment may not be feasible when assembling all of the gratings required for a satellite mission. In that event, optical methods must be developed to achieve spectral alignment. We have developed an alignment approach utilizing a Shack-Hartmann wavefront sensor and diffraction of an ultraviolet laser. We are fabricating the necessary hardware, and will be taking a prototype grating module to an X-ray beamline for performance testing following assembly and alignment.

1. INTRODUCTION

The Arcus mission concept is a soft X-ray spectrograph that could be attached to the International Space Station or flown as a free flying satellite.[16] Arcus seeks to investigate structure formation by observing the warm-hot intergalactic medium in absorption, constrain various models of supermassive black hole feedback, and determine the accretion processes involved in the evolution of young stars. The key lines in the Arcus bandpass are O VII and O VIII (22.6–25 Å), where the proposed mission would have a spectral resolution ($\lambda/\Delta\lambda$) greater than 2000 and an effective area greater than 400 cm^2. The mission concept includes a minimum energy resolution and effective area of 1300 and 130 cm^2, respectively, over the full bandpass of 8–52 Å. These specifications provide an order of magnitude improvement in line detection capability over previous spectroscopic missions as evidenced in Fig. 1.

The Arcus layout is shown in Fig. 2. The optical design consists of three "petals" of silicon pore optics (SPO) modules[4] shown in yellow. Within each petal, there are three radial "sectors" with axial position offsets. Each sector forms an independent telescope focus. Off-plane reflection grating modules are matched to each sector, forming three independent diffracted spectra per petal, for a total of nine diffracted spectra at the focal plane. Separate arrays of CCDs are used to detect the spectra from each petal. The system focal length was limited to five meters in this design due to constraints from the ISS, though this could be extended in a free-flying mission.

The off-plane reflection grating geometry is shown in Fig. 3. Use of off-plane gratings for astronomical spectroscopy has been described extensively over the past several decades.[7,8,14] The basic concept is that the grating grooves are aligned nearly parallel with the incident light, producing diffraction out of the incidence plane in a conical geometry. In order to use off-plane gratings in conjunction with a glancing incidence X-ray telescope, the gratings must also be used at glancing incidence and arranged in an array to intercept the converging telescope beam. To limit aberrations in the spectra, the grating grooves must be radially profiled to match the telescope beam convergence. Co-alignment of the gratings ensures that the diffracted spectra overlap at the focal plane. These two considerations result in a geometry where the grooves all point toward a common point at the focal plane called the hub.[12] The figure of each grating must be flat enough such that alignment tolerances are met over the full grating surface. Finally, the groove facets must be angled (blazed) to enhance

Optics for EUV, X-Ray, and Gamma-Ray Astronomy VII, edited by Stephen L. O'Dell, Giovanni Pareschi,
Proc. of SPIE Vol. 9603, 960315 · © 2015 SPIE · CCC code: 0277-786X/15/$18 · doi: 10.1117/12.2186412

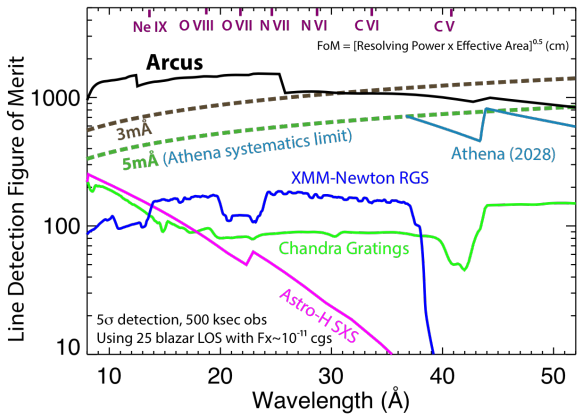

Figure 1. The figure of merit for detecting weak lines is $\sqrt{RE}$, where R is the spectral resolution and E is the effective area. The solid black line shows the prediction for the Arcus mission concept, demonstrating an order of magnitude improvement over previously flown spectrographs.

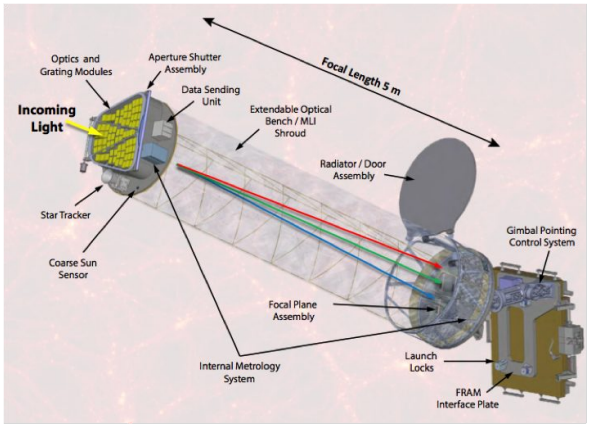

Figure 2. The mechanical design for the Arcus mission concept. Three petals of SPO modules are shown in yellow, with matched off-plane grating modules positioned just below them. The gratings disperse the SPO foci into diffraction arcs at the focal plane. An extendible telescope boom holds the optics at the 5 meter focal length from the focal plane.

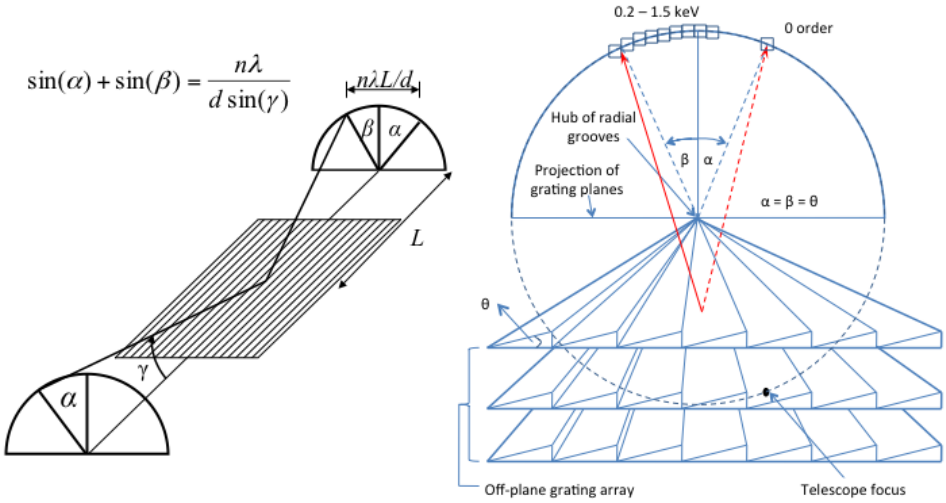

Figure 3. *Left*: Off-plane diffraction occurs with the grooves nearly parallel with the wavevector of the incoming light projected in the grating plane. The light is diffracted out of the incidence plane in what is commonly referred to as conical diffraction. *Right*: The principles of a glancing incidence off-plane grating spectrograph are demonstrated. The grooves must be radially profiled and blazed, and the gratings in an array must be co-aligned such that the grooves all point toward a common hub.

diffraction efficiency to one side of zero order. This increases overall diffraction efficiency and eliminates the need for detectors for both positive and negative diffraction orders.

Alignment sensitivities for the Arcus mission concept are given in Table 1, with the axes defined in Fig. 4. These sensitivities were determined using previously reported raytracing techniques and the nominal Arcus optical design.[1] Translation sensitivities are fairly loose, with the tightest being a 0.2 mm translation along the $\hat{z}$ axis. Alignments of this order of magnitude are easily achieved using modern machining tolerances, meaning the alignment of off-plane gratings in a spectrograph is primarily an angular alignment problem. The sensitivity of

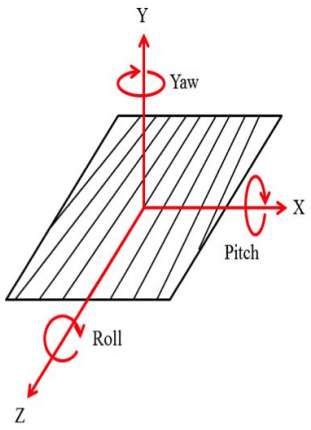

Figure 4. Axis definitions for Arcus grating alignment sensitivities.

Table 1: Arcus Alignment Sensitivities

Axis	Translation	Rotation
$\hat{x}$	± 0.8 mm	± 21.5 arcsec
$\hat{y}$	± 0.5 mm	± 34.5 arcsec
$\hat{z}$	± 0.2 mm	± 5 arcsec

grating roll, or rotation about the $\hat{z}$ axis, is significantly tighter than the other two angular degrees of freedom. This is due to the fact that the spectrograph dispersion direction lies along the axis orthogonal to the groove direction in the plane of the grating. Roll rotations shift the diffraction arc along the dispersion direction, whereas yaw and pitch rotations shift the arc in the cross-dispersion direction. Thus, one must primarily focus minimizing roll variations in grating figure and alignment in order to maintain high spectral resolution.

The Arcus alignment and integration team has developed two approaches to achieving alignment of an off-plane grating module. The first approach is in-situ alignment in a collimated X-ray beam. This approach was tested using a prototype active alignment mount at the MPE PANTER[6] facility in Germany. The second approach is alignment in the laboratory using visible and ultraviolet metrology. We report on the test procedure and results from the in-situ alignment tests at PANTER and on the design of the alternative alignment approach.

2. IN-SITU ALIGNMENT APPROACH

The in-situ alignment approach builds upon methodology developed at the University of Iowa.[2] An alignment mount was fabricated and populated with two off-plane reflection gratings. The first grating was bonded into place to act as a reference grating, while the second grating was adjustable in all angular degrees of freedom using linear actuators. The mount was installed in the PANTER beamline and illuminated with a converging beam from an SPO module. The arcs of diffraction from the two gratings were measured using a large area detector. CCDs were then used to monitor the diffraction arcs as the active grating was aligned to the reference grating. After alignment, the active grating was bonded into place and the spectral alignment of the resulting spectrograph was verified. Reports on spectrograph performance and replicated gratings tested during this campaign are reported in companion papers.[10,13]

2.1 Active Alignment Module

The active alignment mount (AAM) is shown in Fig. 5. Gratings are inserted into the module between precision bosses that define their nominal positions. The first grating inserted into the module is bonded to its set of bosses and acts as a reference grating. Each subsequent grating is installed into the next set of bosses for alignment with respect to the previous grating. The gratings are manipulated using five Newport 8310 Picomotor actuators with a ~ 30 nm stepsize, providing ~ 0.06 arcsecond angular steps. Springs opposite each actuator head provide the force necessary to maintain contact with the actuators. A software interface written in LabVIEW is used to control the actuators via TCP/IP communication.

2.2 Gratings

Two identical gratings were used for the alignment tests. They were purchased from LightSmyth and were fabricated using deep UV reduction lithography and reactive ion etching. The groove profile is laminar with an

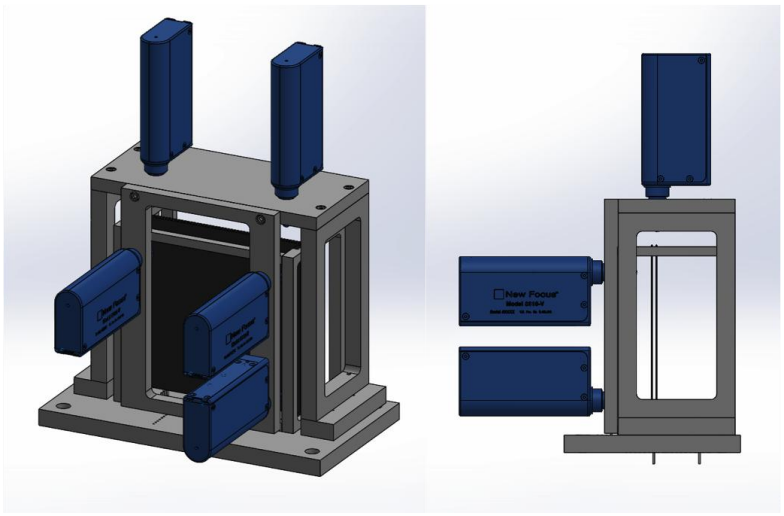

Figure 5. The mechanical design of the active alignment mount. Five Newport 8310 Picomotor actuators are used to manipulate the active grating. The two actuators at top are used to control the grating yaw, and the three actuators facing the grating normal are used to control pitch and roll. A spring is positioned opposite each actuator to maintain a normal force against the actuator.

average 166 nm period (6033 lines/mm). The groove pattern is a radial approximation, where the groove period decreases in two discrete steps (three total sections with 6024, 6033, and 6042 lines/mm) along the axial length of the grating. Both gratings are shown in the AAM in Fig. 6. Protective wafer tape can be seen covering the gratings with the exception of the 25 x 32 mm^2 central, active areas. The gratings are bare silicon, without any reflection enhancing coating.

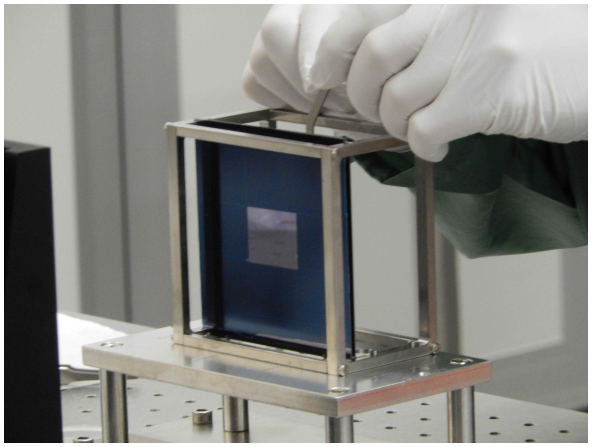

Figure 6. The active alignment mount being populated with gratings. The active grating is shown in front of the previously bonded reference grating. Springs are in the process of being inserted to provide a normal force to the active grating. The wafer tape masks all but the central, active area of the gratings.

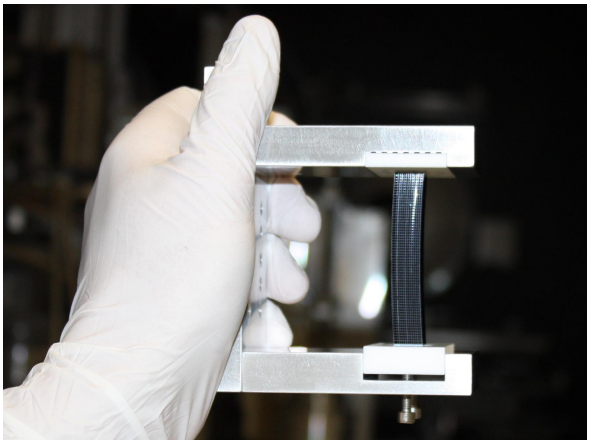

Figure 7. A view of the silicon pore optic module prior to installation into the beam line. The azimuthal direction is vertical and the radial direction is horizontal.

2.3 SPO Module

Silicon pore optics, developed primarily by cosine Research, have been baselined for the Arcus mission concept as the imaging optics. They are also the driving optics technology behind the upcoming Athena mission.[18] The

fabrication of SPOs involves standard techniques from the electronics semiconductor industry. The reflecting surfaces consist of super polished silicon wafers cut into the desired rectangular shape. Each wafer is wedged to account for the fan angle between adjacent reflective surfaces in a nested Wolter-I telescope.[17] A reflective coating is applied in strips to the front side, and the back side is diced to leave ribs to act as spacers between surfaces. The wafers are stacked together with precision robots, and the silicon ribs form covalent bonds with the uncoated wafer surfaces with which they make contact. The result is a monolithic conical approximation of a Wolter-I telescope made entirely of silicon, with pores through which X-rays may propagate. Separate stacks are made for the primary and secondary reflecting surfaces, which are then bonded into an assembly using a silicon carbide bracket.

The SPO module used in this test consists of 13 plates with an inner and outer azimuthal radius of curvature of 439 mm and 450 mm, respectively. The module is 66 mm wide in the azimuthal direction and 22 mm long in the axial direction. Due to cost and schedule considerations, only the primary surface was included in this SPO module. The stacking robot used to fabricate this module was designed for mirrors with larger radii of curvature, and an aluminum mandrel was used to stack the wafers rather than a high quality fused silica mandrel. Thus, the angular resolution of this SPO module was worse than state-of-the-art modules being produced by cosine.[9] The focal length for the primary surface was nominally 8 m, though the effective focal length given the finite PANTER source distance was measured to be ~ 8.5 m. For these tests, a mask was used to restrict the SPO illumination to $\sim 66\%$ of the azimuthal span.

2.4 Test Setup

Fig. 8 presents the test geometry. The SPO module was illuminated and characterized prior to installation of the AAM into the beamline test chamber. The AAM was installed roughly 500 mm from the SPO module on a stack of translation and rotation stages. These stages provided translation in and rotation about the $\hat{x}$ and $\hat{y}$ axes. These rotations correspond to yaw and pitch in Fig. 4. The roll angle of the AAM was not crucial for the alignment purposes of the test, and was set by mechanical tolerances. The pitch angle was set by monitoring the separation of the telescope focus and the specularly reflected zero order beam at the focal plane while illuminating the SPO module and AAM with a collimated alignment laser as shown in Fig. 9. Because the two gratings only intercept a small fraction of the SPO beam, both spots were simultaneously visible at the focal plane, and the pitch angle of the AAM was adjusted to achieve a 1.50 ± 0.07 degree incidence angle.

After pitch alignment of the AAM, the chamber was pumped down to vacuum and the electron impact source with a Mg target turned on. The yaw angle of the AAM was set to zero by adjusting the $\hat{y}$ positions of the $\pm$1st order Mg K lines to be equal. This was done using the TRoPIC CCD, which is a prototype of the eROSITA detector.[15] The ROSAT position sensitive proportional counter (PSPC) flight spare was then scanned over the diffraction arcs from the two gratings.[5] This detector was used to form a mosaic image of the diffraction arcs due to its large field-of-view. One side of the mosaic is shown collapsed in the cross-dispersion direction in Fig. 11 to display the prominent lines seen in the diffracted spectra.

2.5 Co-Alignment Procedure and Results

With the AAM aligned to the converging X-ray beam, the process of aligning the active grating to the reference grating was accomplished by using the zero order specular reflection and first order Mg-K line of each grating. TRoPIC was positioned to monitor the zero order reflections as the pitch and roll of the active grating was adjusted. The goal was to achieve the best overlap by minimizing the RMS spread of the co-aligned zero order spots in both the dispersion and the cross-dispersion directions. For pitch alignment, the pitch actuator was adjusted by 100 actuator steps (~ 6 arcseconds) per scan step and the RMS spread recorded at each scan step. The point spread functions (PSFs) at both the start of the scan and the position of best alignment are shown in Fig. 12. The exact same procedure was carried out for roll alignment, with the results shown in Fig. 13.

It is possible to achieve extremely precise alignment of zero order reflections in an off-plane grating array while the diffracted spectra are still grossly misaligned. Residual misalignment would be due to yaw misalignments of the gratings, which cause a pseudo-rotation of the diffraction arc about the zero order reflection (see Ref. 1 for details). To ensure there were no residual yaw misalignments, TRoPIC was positioned to monitor the 1st order Mg-K line. Separation of the diffracted spots from each grating were observed in the cross dispersion direction

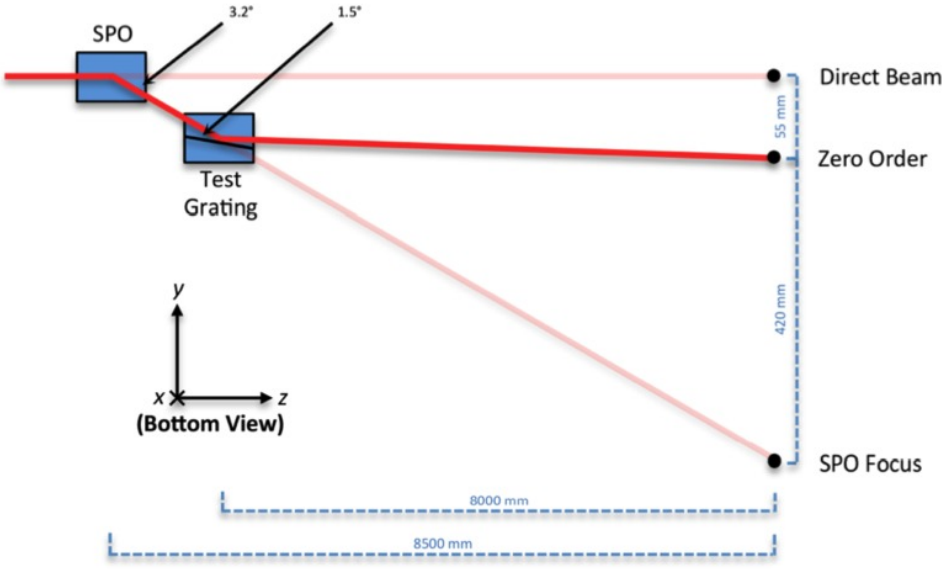

Figure 8. A schematic of the in-situ alignment test at the PANTER facility. Gravity is in the $\hat{x}$ direction. Figure is not to scale.

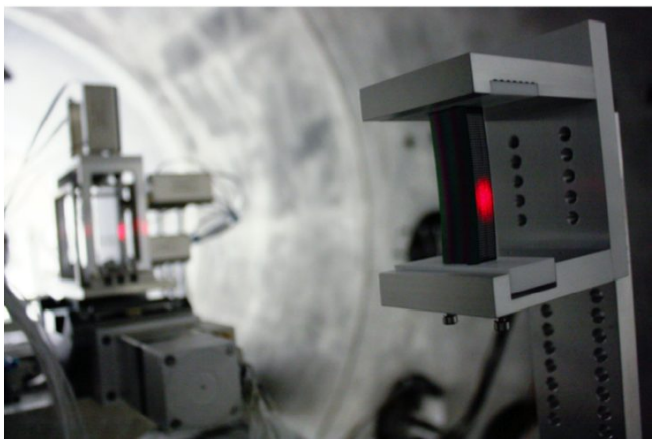

Figure 9. A view of the SPO module and the AAM during coarse alignment to the PANTER optical axis. A collimated alignment laser is used to set the position and incidence angle of the AAM.

as shown in Fig. 14. One of the two actuators used to control the active grating yaw alignment failed during the test, which prevented optimal alignment in this degree of freedom. The functioning yaw stage was completely disengaged from the active grating, which improved the alignment as shown in Fig. 15. To continue aligning the Mg-K spots to one another, the other stage needed to be driven, which was not possible. Analysis of the PSF centroids in Fig. 15 yields an estimated residual yaw misalignment of 16.6 arcminutes. As reported previously,[1] yaw misalignments primarily affect the spread of spectra in the cross-dispersion direction, which has little effect on the spectral resolution over the co-aligned arcs. Raytracing the yaw misalignment indicates that it should contribute less than 16 μm (0.4 arcseconds) of spread in the dispersion direction at 3rd order Mg-K and even less at lower dispersion lines. Given that this is a small fraction of the spectrograph LSF (see below), the yaw alignment had a negligible effect on the achieved spectral alignment of the gratings for the bandpass tested.

To check the quality of the spectral alignment, the line spread function (LSF) was measured at three distinct regions in the spectrum. The zero order specular reflection, the 1st order Mg-K line, and the 3rd order Mg-K

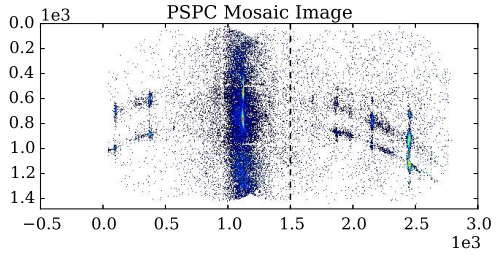

Figure 10. A mosaic image of the two diffraction arcs from the initially misaligned gratings in the AAM. The region to the right of the vertical dashed line indicates the region shown in the collapsed spectrum in Fig. 11.

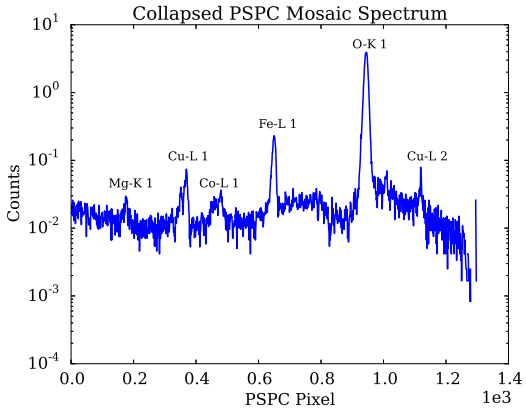

Figure 11. The region to the right of the dashed line in Fig. 11 is shown collapsed in the cross-dispersion direction. The prominent spectral lines from the Mg target in the X-ray source are indicated.

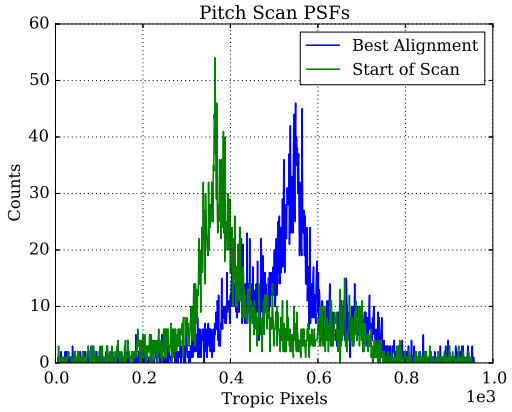

Figure 12. The combined point spread functions of the active and reference grating zero order reflections. The PSF at the start of the alignment scan is shown in green, with the central peak of the active grating PSF displaced to the edge of that of the reference grating. In blue, the optimally aligned combined PSF is shown. The central peak of the active grating PSF lies roughly in the center of the broader reference grating PSF.

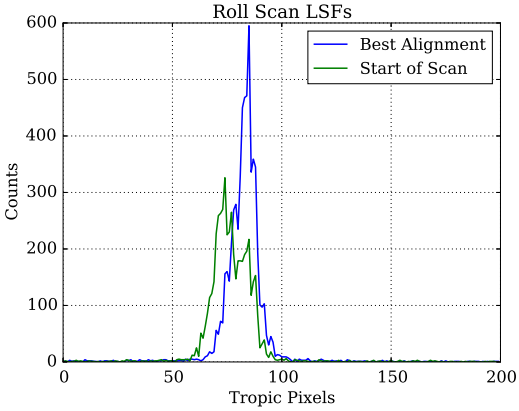

Figure 13. The combined line spread functions of the active and reference grating zero order reflections. The LSF at the start of the alignment scan is shown in green, and is clearly broader than the optimally aligned LSF shown in blue.

line were all investigated. For logistical reasons, the Mg-K LSFs were measured with the Princeton Instruments PI-MTE-1300B CCD. The half energy width (HEW) was used as a figure of merit due to the non-Gaussian shape of the LSFs. A rotation was applied to the line images in order to minimize the spread in the dispersion direction. This technique accounts for a potential rotational misalignment of the detector in the xy plane (Fig. 8). The optimally rotated lines were then collapsed in the cross-dispersion direction, and the counts then cumulative summed into a normalized cumulative distribution function (CDF). A spline fit was made to the CDF and the HEW was taken by finding the difference between the positions of the 75th and 25th CDF percentiles.[13] The PSF of the zero order and the LSFs of the 1st order Mg-K and 3rd order Mg-K lines were 2.70 arcseconds, 2.01 arcseconds, and 2.82 arcseconds, respectively. The natural width of Mg-K (0.36 eV) corresponds to a maximum resolution of $\sim$ 3500. The achieved resolutions of 628 and 1373 at 1st and 3rd order indicate that the Mg-K natural width has a negligible impact on spectral resolution (i.e. the observed widths are significantly broader than the natural line width). The remaining lines have broader natural widths that require more careful analysis.

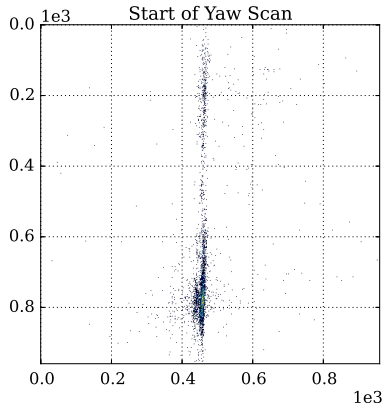

Figure 14. Images of the 1st order Mg-K line from the active and reference gratings at the beginning of the yaw alignment scan. The line from the active grating is on the bottom of the image, and is displaced from that of the reference grating due to a yaw misalignment of the active grating.

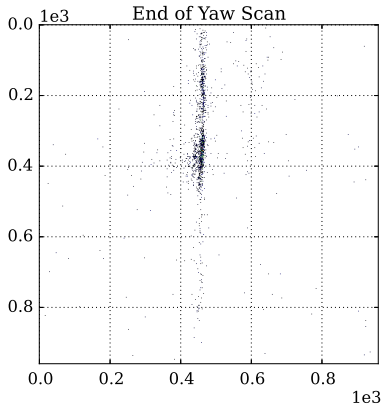

Figure 15. Images of the 1st order Mg-K line from the active and reference gratings at the end of the yaw alignment scan. Due to failure of one of the two yaw actuators, the misalignment was not completely correctable. The line from the active grating is significantly closer to that of the reference grating as compared to Fig. 14.

For the lines analyzed, no significant degradation of resolution from the zero order performance is observed.

The chamber was vented and the active grating was bonded into place using Appli-tec 5200 epoxy. After a 24 hour curing period, the actuators were disengaged from the grating and the springs removed from the system. The chamber was pumped back down to vacuum and the HEW of the 1st order Mg-K line was measured to detect a misalignment due to bonding. The post-bonding 1st order Mg-K HEW was measured to be 1.97 arcseconds. This measurement is clearly consistent with no induced spectral misalignments during the bonding and curing process.

Several important lessons can be drawn from this alignment test. The spectral alignment of the grating array was checked from zero order out to 3rd order Mg-K (equivalent 2.97 nm wavelength in 1st order), but the Arcus bandpass would extend farther out along the arc. The Arcus 1st order bandpass ranges from 2.5 to 5.1 nm, and it would be necessary to use lines in this bandpass as metrics during the alignment process. Otherwise, alignment could be optimized in a non-critical portion of the diffraction arc while being slightly degraded in the bandpass of interest. It is also essential to have naturally narrow spectral lines with which to do the alignment in this bandpass. Narrow lines will provide the tightest spectral LSF, which represents a limit on the ultimate accuracy of in-situ alignment of off-plane gratings. In fact, even with an infinitely narrow spectral line, the LSF of the telescope feeding the grating array limits the accuracy of spectral alignment. The Arcus grating alignment requirement is 5 arcseconds for the roll rotation, which equates to 0.1 arcsecond shifts in the dispersion direction at the focal plane due to the glancing incidence geometry. With a ~ 2 arcsecond telescope LSF, such misalignments would be very difficult to measure. It is clear that very long exposures are necessary to confirm alignment tolerances that are only a fraction of the spectrograph LSF. Finally, and perhaps most importantly, the process of in-situ X-ray alignment is very expensive both in terms of cost and schedule.

3. LABORATORY ALIGNMENT APPROACH

To circumvent the challenges and limitations of in-situ X-ray alignment, the Arcus collaboration has developed a laboratory approach for the population and alignment of an off-plane grating module. In this approach, gratings are inserted into a module and manipulated with a hexapod prior to bonding. During manipulation, the alignment of a grating is monitored with both visible and ultraviolet metrology systems. The overall strategy, mechanical design, and metrology systems are described below.

3.1 Alignment Strategy

A conceptual diagram of the laboratory alignment approach is shown in Fig. 16. A Shack-Hartmann wavefront sensor (WFS) system previously developed for the SAO adjustable X-ray optics program[3] is used to monitor the pitch (rotation about $\hat{x}$), roll (rotation about $\hat{z}$), and figure of a grating during alignment. A 266 nm collimated ultraviolet laser is used to monitor grating yaw (rotation about $\hat{y}$), to which the WFS is insensitive. This technique is based on the grating period uniformity measurements on the high energy transmission gratings for the Chandra Observatory.[11] The UV laser is used in the in-plane diffraction geometry, where both a specularly reflected beam and a Littrow back-diffracted beam are produced at an incidence angle of $\sim 35°$. For practical purposes, the laser will be shifted a few degrees out of the Littrow configuration to permit the placement of a CMOS detector to monitor the location of the diffracted spot. Under small yaw rotations, the diffracted spot will shift in the $\hat{z}$ direction, providing feedback on the grating yaw angle. An additional CMOS camera will be used to monitor the reflected spot, providing redundant feedback on the grating pitch and roll angles.

Fig. 17 shows the mechanical design of the grating module. The housing is made from titanium, primarily for mass and stiffness considerations. The grating substrates are fused silica, which has a coefficient of thermal expansion (CTE) mismatch with the titanium. To alleviate thermal issues, carbon-fiber inserts are used as an interface material between the gratings and the housing. The carbon-fiber can be fabricated to have a CTE matched to that of the fused silica. Flexures are machined into the titanium housing and the carbon-fiber inserts bonded to them. Flexures are bonded to the edge of the grating substrate prior to the alignment within the module and then bonded to the carbon-fiber insert during alignment (see Fig. 18). Bonding to the carbon-fiber insert is accomplished through fused silica bonding rods used to transmit UV light during epoxy cure. There is a cutout near one axial edge of the housing to permit the UV yaw alignment laser to access all of the gratings as the module is populated. The module is designed to hold 15 individual gratings. Due to the Arcus focal length, there is a nominal 2.2 arcminute fan angle in the pitch direction between adjacent gratings.

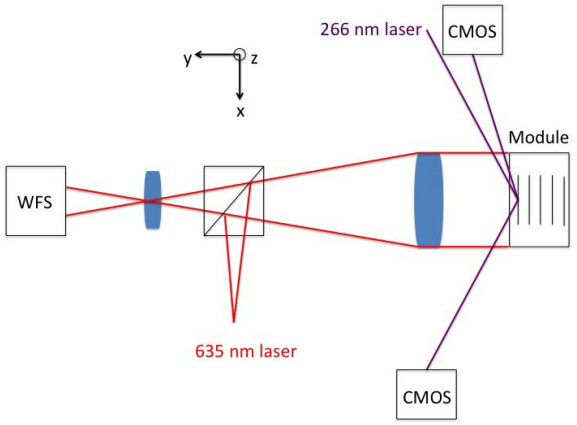

Figure 16. A conceptual diagram of the laboratory off-plane grating alignment approach developed for the Arcus mission concept. Grating figure and both pitch and roll alignment are monitored with a wavefront sensing system. Grating yaw is monitored with a UV laser system. The module is indexed on a movable platform such that gratings are always installed and aligned at the same physical position with respect to the metrology.

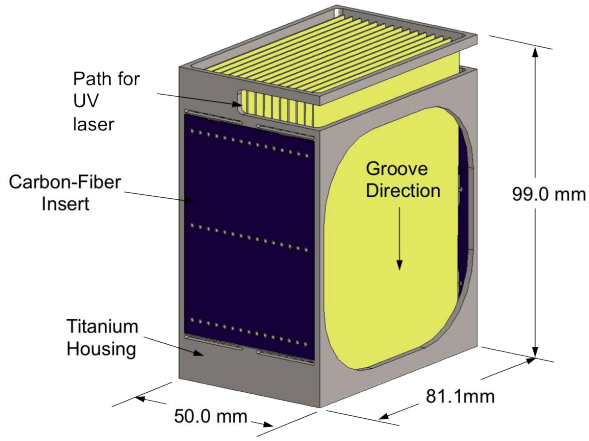

Figure 17. The mechanical design of the laboratory alignment module. The nominal X-ray path is vertical as indicated by the groove direction vector. The module is made of titanium with flexures machined into the structure. Carbon-fiber inserts on either side of the module are bonded to the titanium flexures. Flexures are bonded to grating substrates which are then inserted and aligned within the module. Gratings are bonded to the carbon-fiber inserts through fused silica rods which transmit UV light for epoxy curing.

The alignment procedure begins with using an optical reference flat to calibrate the WFS for figure measurement. The grating module is then moved into position for installation of the first grating at the back of the module as seen from the WFS (i.e. the grating farthest to the left in Fig. 17). Alignment of the UV laser and the CMOS cameras is then carried out such that the diffracted and reflected spots are roughly in the center

of the detectors. The CMOS cameras are positioned roughly 200 mm from the beam impact location. After the first grating is bonded into place, the WFS signal and CMOS images are saved to be used as references for the subsequent grating alignment. The entire grating module is then indexed such that the next grating is inserted into the exact same location relative to the metrology systems as the previous grating. This is achieved using mechanical tolerances for translations and the WFS signal for pitch and roll. The WFS system has a large enough depth-of-field and dynamic range that it can verify the 2.2 arcminute pitch rotation of the first grating as the module is indexed. An optical reference flat is fixed to the indexing platform to which the grating module is attached to act as a global yaw angle reference. A theodolite is used to verify that the yaw angle of the module is not misaligned during the indexing process. After the indexing is complete, the next grating is inserted into the module and attached to a hexapod for alignment. The grating is manipulated until the tip and tilt of the WFS measurement matches that of the previous grating, and the diffracted and specular UV spots are at the same location as those of the previous grating. This ensures that this grating is aligned to the same physical location as that of the previous grating prior to module indexing. Thus, accurate relative grating positions are achieved by accurate grating module indexing. This process proceeds iteratively until the entire module is populated. The WFS measurement for each grating is referenced to the optical flat for figure measurements.

Figure 18. The mechanical design of the grating substrate with flexures bonded to the edges. These flexures are used for bonding the gratings to the carbon-fiber inserts shown in Fig. 17.

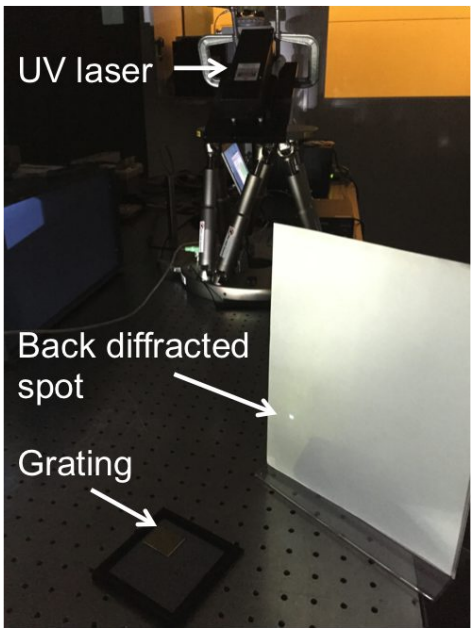

Figure 19. A 266 nm UV laser is positioned on a hexapod and directed toward a laminar grating positioned on the optics bench. This grating has a 166 nm groove period which produces a bright back-diffracted beam.

3.2 Initial Tests

The UV alignment metrology is a novel approach for off-plane grating alignment, prompting initial feasibility tests with a 266 nm collimated laser module. A laminar grating with a 166 nm groove period (as with the in-situ alignment gratings) was illuminated with the laser in order to test for the presence of back diffraction. The experimental setup is shown in Fig. 19. The laser module was positioned on a hexapod platform and pointed toward the grating resting on the optics bench. The grating was given a significant yaw angle in order to direct the diffracted beam out of the path of the incident beam. A plastic sign holder with a white piece of paper was placed in the diffracted beam's path. The fluorescence due to the diffracted spot can clearly be seen in the photograph. Note that this laser tends to fluoresce off most materials, making it nearly as easy to work with as a visible laser. The alignment of this setup was done by eye and is not precise.

Windowless CMOS cameras were also procured to detect the UV laser beam. The hexapod was used to

provide a 600 μm lateral shift to the laser module while the direct output of the beam was monitored with one of the cameras. Using only the central slices of the images taken before and after translation, the shift of the centroid was recovered to an accuracy of 20 μm. Given that a 30 arcsecond yaw misalignment of an Arcus grating would result in a 60 μm shift of the diffracted spot during alignment, this accuracy is more than adequate. It should also be possible to significantly improve centroiding accuracy by using refined analysis of the entire image rather than only the central slices.

4. SUMMARY AND FUTURE PLANS

We have tested an in-situ alignment approach for a pair of off-plane reflection gratings in the path of a converging X-ray beam from an SPO module. The results from the test confirmed our understanding of the general approach and the effects of the various degrees of freedom. Due to the broad LSF of the spectrograph, we were unable to demonstrate spectral alignment to within the tolerances required by the Arcus mission concept. Various other challenges and limitations of in-situ alignment were highlighted through this experiment, motivating the development of a laboratory alignment approach using visible and UV metrology. We have designed an overall alignment and metrology strategy and are in the process of fabricating parts. We will populate a prototype module with co-aligned gratings and test this module in an X-ray facility. Our goal is to acquire long enough exposures to statistically prove co-alignment within the Arcus tolerances.

ACKNOWLEDGMENTS

This work was supported by a NASA Strategic Astrophysics Technology grant (NNX15AC42G) and a NASA Astrophysics Research and Analysis (APRA) grant (NNX13AD03G). This work was also supported by internal funding from the Smithsonian Astrophysical Observatory, a bureau of the Smithsonian Institution.

REFERENCES

[1] Allured, R., & McEntaffer, R. T. 2013, Experimental Astronomy, 36, 661
[2] Allured, R., Donovan, B. D., & McEntaffer, R. 2013, Proc. SPIE, 8861, 88611C
[3] Allured, R., Cotroneo, V., Johnson-Wilke, R., et al. 2014, Proc. SPIE, 9144, 91441D
[4] Beijersbergen, M., Kraft, S., Gunther, R., et al. 2004, Proc. SPIE, 5488, 868
[5] Briel, U. G., & Pfeffermann, E. 1986, Nuclear Instruments and Methods in Physics Research A, 242, 376
[6] Burwitz, V., Bavdaz, M., Pareschi, G., et al. 2013, Proc. SPIE, 8861, 88611J
[7] Cash, W. C., Jr. 1983, App. Opt. 22, 3971
[8] Cash, W. C., Jr. 1991, App. Opt. 30, 1749
[9] Collon, M. J., Ackermann, M., Günther, R., et al. 2014, Proc. SPIE, 9144, 91442G
[10] DeRoo, C. T. et al. 2015, Submitted to SPIE JATIS.
[11] Dewey, D., Humphries, D. N., McLean, G. Y., & Moschella, D. A. 1994, Proc. SPIE, 2280, 257
[12] Flanagan, K. A., Davis, J. E., Heilmann, R. K., et al. 2004, Proc. SPIE, 5488, 515
[13] Marlowe, H., McEntaffer, R. L., Allured, R., et al. 2015, Proc. SPIE, 9510, 95100O
[14] McEntaffer, R. L., Murray, N. J., Holland, A., et al. 2009, Proc. SPIE, 7437, 74370H
[15] Meidinger, N., Andritschke, R., Ebermayer, S., et al. 2009, Proc. SPIE, 7435, 743502
[16] Smith, R. K., Ackermann, M., Allured, R., et al. 2014, Proc. SPIE, 9144, 91444Y
[17] van Speybroeck, L. P., & Chase, R. C. 1972, App. Opt. 11, 440
[18] Willingale, R., Pareschi, G., Christensen, F., et al. 2014, Proc. SPIE, 9144, 91442E